Neurospine 2026;23(1):187-201.
https://doi.org/10.14245/ns.2551470.735

Neurospine
pISSN 2586-6583 eISSN 2586-6591

Original Article

Biomechanical Analysis Comparison of Different Cervical Posterior Screw Fixation Techniques: A Finite Element Study

Corresponding Author
Byung Ho Lee
https://orcid.org/0000-0001-7235-4981

Department of Orthopedic Surgery, Yonsei University College of Medicine, 50 Yonsei-ro, Seodaemun-gu, Seoul 03722, Korea
Email: bhlee96@yuhs.ac

Received: October 7, 2025
Revised: December 2, 2025
Accepted: December 12, 2025

Joonoh Seo[1,2,*], Woo-Seok Jung[3,*], Tae Hyun Park[4], Sung-Jae Lee[4], Ji-Won Kwon[1], Kyung-Soo Suk[1], Byung Ho Lee[1]

[1]Department of Orthopedic Surgery, Yonsei University College of Medicine, Seoul, Korea
[2]Department of Orthopedic Surgery, Ewha Womans University Seoul Hospital, Seoul, Korea
[3]Pohang Yonsei Orthopedic Clinic, Pohang, Korea
[4]School of Biomedical Engineering, Inje University, Gimhae, Korea

*Joonoh Seo and Woo-Seok Jung contributed equally to this study as co-first authors.

Objective: To biomechanically compare the stress distribution of established posterior cervical fixation techniques—conventional pedicle screw (PS), Abumi technique, unicortical lateral mass screw (LMS), and bicortical LMS—with a novel PS method, the Lee point technique, using finite element modeling (FEM).
Methods: A patient-specific FEM of C5–6 was developed using high-resolution computed tomography scan data of a degenerative cervical spine. Five fixation models were constructed: Lee point, Abumi, conventional PS, unicortical LMS, and bicortical LMS. Screw dimensions were ø3.5 × 28 mm for PS and ø3.5 × 14/18 mm for LMS. A pure moment of 1.0 N·m was applied in flexion, extension, axial rotation, and lateral bending, and the peak von Mises stress (PVMS) of both the vertebrae and implants was recorded for each loading condition.
Results: Abumi technique showed the highest PVMS at C5–6 (23.09–43.22 MPa and 24.96–39.91 MPa), with stress concentrated at the pedicle entry and medial wall. Lee point and conventional PS demonstrated more evenly distributed stress across the pedicle and near cortex of the lateral mass. Unicortical and bicortical LMS showed stress mainly at the entry point, with overall lower and more uniform magnitudes. Implant stress was greatest in Abumi construct (up to 295 MPa), moderate in Lee and conventional PS, and lowest in LMS models.
Conclusion: Abumi technique showed higher localized stress concentrations that may warrant careful patient selection, particularly in those with compromised bone quality. Lee point technique achieved a balanced stress profile comparable to conventional PS, suggesting a favorable biomechanical profile for posterior cervical fixation.

Keywords: Cervical spine, Pedicle screws, Lateral mass screw, Finite element analysis

INTRODUCTION

With the rising burden of cervical degenerative disease, trauma, inflammatory or infectious conditions, and neoplastic disorders, posterior cervical spine fixation has become a widely adopted surgical strategy.[1-3] Recent advancements in navigation technology have enhanced the safety of cervical pedicle screw (PS) placement, resulting in a growing adoption of this technique in clinical practice.[4-6] Among the available techniques, lateral mass screw (LMS) fixation and cervical PS fixation are commonly used.[7-10] LMS placement can be performed using either unicortical or bicortical purchase,[11] while PS insertion techniques include the conventional cervical PS method, Abumi technique, and the medial pedicle pivot point technique

(Lee point technique) which is known to be safer method compared to conventional.[12-15]

Several studies have compared the safety and pullout strength of unicortical and bicortical LMSs.[11,16,17] Similarly, comparative studies have also been conducted between the Abumi technique and the conventional PS method.[18-20] Although prior biomechanical studies have investigated the fixation strength of lateral mass versus PSs, as well as unicortical versus bicortical LMSs, comprehensive comparisons of stress distribution patterns among all these techniques using finite element (FE) analysis are lacking.[21-24]

FE modeling (FEM) provides a powerful means to evaluate construct biomechanics under well-controlled, physiologic loading scenarios.[25,26] Building on this rationale, the present study analyzes and compares the stress-distribution characteristics of commonly used posterior cervical fixation strategies—conventional cervical PS, Abumi technique, Lee point technique, unicortical LMS, and bicortical LMS —within a single FEM platform. By quantifying peak von Mises stress (PVMS) across clinically relevant loading modes, we aim to clarify technique-specific stress patterns that may have implications for construct safety and durability.

MATERIALS AND METHODS

1. Procedure of Patient-Specific FEM

The geometry and dimensions of the model were obtained from a high-resolution computed tomography (CT) scan data of a subject with spinal pathology were used (female, 49 years with osteopenia). DICOM images were imported into Mimics image processing and editing software (Materialise, Belgium) for segmentation. Since soft tissue was poorly visualized on CT scans, the discs were generated using the wrap function in 3-matics (Materialise). Discs were modeled as a composite of a solid matrix based on the surface of intervertebral endplate. The FE mesh was generated using in 3-matics (Materialise).

2. Intervertebral Disc Material Properties

The intervertebral disc between C5 and C6 was modeled as a solid composite structure consisting of the annulus fibrosus and the nucleus pulposus. Because CT data did not clearly delineate the soft tissue boundaries, the disc geometry was reconstructed using the wrap function in 3-matic and assigned homogeneous isotropic material properties based on previously published FE models of the human intervertebral disc (Young modulus of 1.0 MPa and a Poisson ratio of 0.49).[27]

3. Material Assignment

The 3-dimensional mesh was exported from 3-matics and imported again into Mimics where the element stiffness was assigned using the Hounsfield values from the CT scans. It has been reported that discrepancy in accuracy can lie in how the Young modulus of each element is space between calculated and missing.[28] In general, material assignment for voxels within CT scans is based on averaging the Hounsfield units of each pixel inside each element. This method could give poor results should the element size be larger than the voxel. Therefore, it was attempted to have the element size smaller or similarly sized as the voxels in order to minimize errors.

Previously published papers have addressed the relationship between the Hounsfield values and the density.[29] It was assumed that the density was related to the Hounsfield units, using the expression obtained from Rho et al.[30]

$$\text{Eq(1)}\rho = -13.4+1017\ \text{HU (Hounsfield unit)}\ (\text{g/cm}^3)$$

The material properties were applied on the FE mesh, using the Mimics software where an average Young modulus was calculated from the CT Hounsfield value. Experimental data have shown that a power law exists between the Young modulus and the apparent density. In an *in vitro* study of the bone mechanical properties carried out by Rho et al.,[30] three different density-stiffness expressions were applied to a FE model of the spine and strain results were compared to experimental values. It was found that the material expression that best agreed with the experimental values was:

$$\text{Eq(2)}\ E = -349+5.82\rho\ (\text{MPa})$$

4. Postoperative Modeling

The surgical model was reconstructed by measuring the lordotic angle and disc height based on the lateral view x-ray image (AutoCad LT 2020, USA) of an actual patient after surgery. At this time, the disc was reconstructed base on the changed position (Supplementary Fig. 1) OCT spinal fixation system (Poseidon, Medyssey Co. Ltd., Korea) was implanted following each surgical technique (C5–6).

Surgical models can be divided into the PS technique and the LMS technique. For the PS technique, Lee point technique, Abumi technique, and the conventional PS technique were applied. Despite applying the specific characteristics of each PS technique, the screw positions were kept identical. In this case, ø3.5×28-mm implants were used.[12-15] For the LMS, an LMS unicortical screw (ø3.5×14 mm), which fixes only the entry cortical bone, and an LMS bicortical screw (ø3.5×18 mm), which

https://doi.org/10.14245/ns.2551470.735

fixes both the entry and far cortical bone, were constructed. In the model construction process, the screw positions were determined based on clinical judgment, with the entry point and trajectory being applied consistently for all screws[15] (Fig. 1).

5. Loading and Boundary Conditions

A surface-to-surface contact was defined between vertebral body and screw body with friction coefficient of 0.3, and for other structures was defined bond contact condition. All nodal points of lower endplate of the C6 were fixed, while the upper endplate of the highest segment was subjected to a pure moment of 1.0 N·m of flexion, extension, axial rotation, and lateral bending, combined with a compressive preload of 73.6 N.[31] The applied load magnitude of 1.0 N·m was selected according to established experimental and FE standards for physiological cervical spine motion. Previous cadaveric studies have demonstrated that a pure moment of approximately 1 N·m produces normal ranges of motion in the subaxial cervical spine without inducing structural damage.[32,33] Accordingly, most subsequent FE models have adopted this load magnitude for comparative anal-

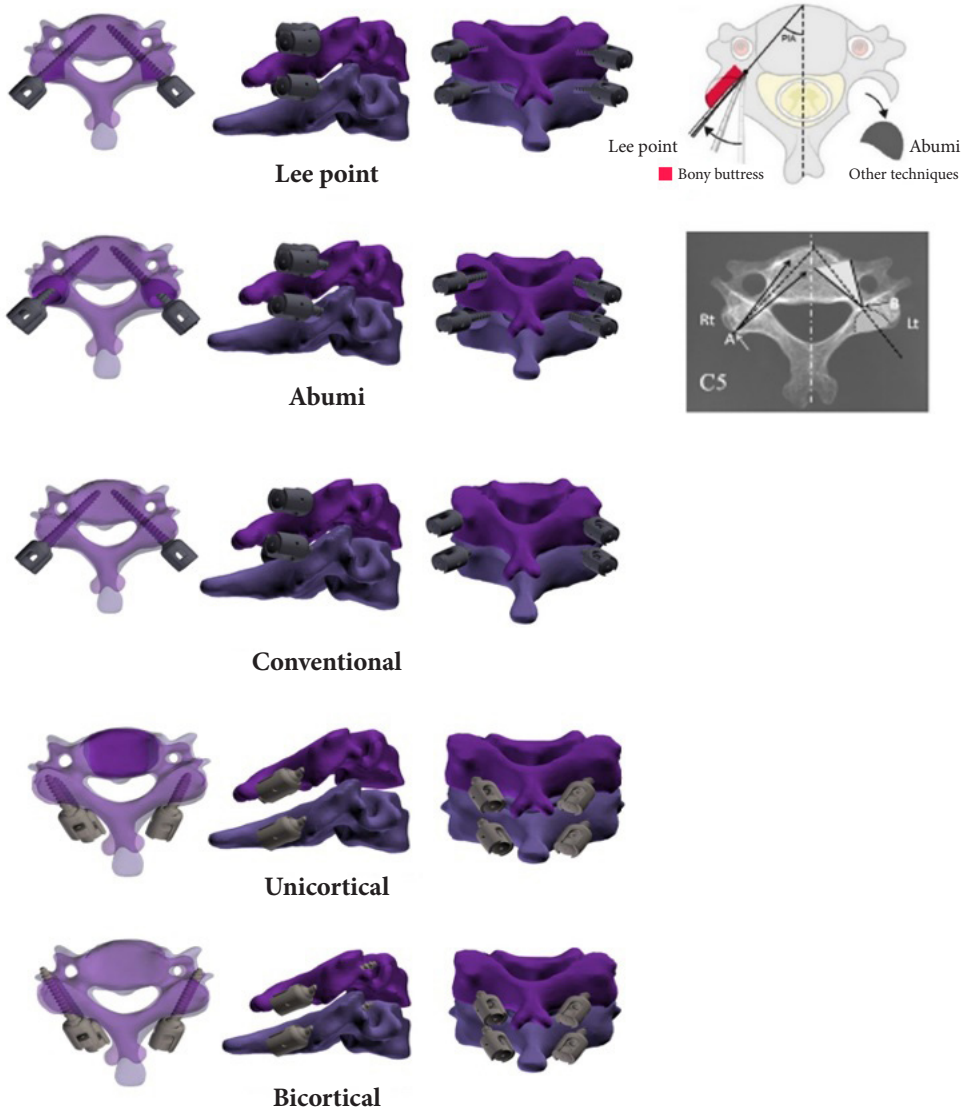

Fig. 1. Surgical models; Lee point technique, Abumi technique, Traditional pedicle screw technique, unicortical lateral mass screw, bicortical lateral mass screw. Bone removal according to each technique is illustrated, with the resected portion highlighted in dark purple. In Lee point technique, the medial portion of the lateral mass is removed while preserving the lateral part.[15] In the Abumi technique, a substantial portion of the lateral mass is removed to identify the screw entry point.[14] In the conventional technique, no part of the lateral mass is resected.[12] Both unicortical and bicortical lateral mass screws were applied according to the referenced technique(s).[11]

ysis of cervical fixation biomechanics.[21,22] The PVMS of the vertebral body and implant in each of the different model were recorded for each loading condition. The interaction stress, occurring between the inter segment during each physiological loading. This research used ABAQUS (Dassault Systems, France).

6. FEM Validation

In this study, model validity was assessed based on the anterior-posterior load-sharing ratio. Load-sharing was estimated from nodal force measurements, and the corresponding anterior-posterior ratio was calculated. The predicted results were then compared with those from previous studies[34] to verify the contribution of posterior load-sharing.

7. Ethics Statement

The study protocol was approved by the Institutional Review Board of Yonsei University College of Medicine (2025-0903-001), and the requirement for informed consent was waived due to the retrospective use of de-identified imaging data.

RESULTS

1. PVMS at C5

The PVMS at the C5 vertebra under four principal motion conditions—flexion, extension, axial rotation, and lateral bending—was evaluated across 5 posterior fixation techniques: Lee point technique (Lee), Abumi PS technique (Abumi), conventional PS (Pedicle), unicortical LMS (Uni-LMS), and bicortical LMS (Bi-LMS).

In flexion, PVMS values were 9.14 MPa (Lee), 23.09 MPa (Abumi), 7.51 MPa (Pedicle), 7.80 MPa (Uni-LMS), and 8.03 MPa (Bi-LMS). Abumi showed the greatest stress concentration with vivid high-stress zones at the screw entry point and along the medial pedicle wall. In contrast, Lee, Pedicle, and both LMS models exhibited more uniform distributions without focal hotspots. Uni- and Bi-LMS demonstrated low-moderate stress along the lateral mass trajectory; Bi-LMS displayed a slightly broader spread toward the far cortex without evidence of overload (Figs. 2 and 3).

In extension, PVMS was 9.57 MPa (Lee), 31.96 MPa (Abumi), 8.19 MPa (Pedicle), 7.82 MPa (Uni-LMS), and 8.63 MPa (Bi-LMS). Abumi again produced the highest stress, with red zones at the pedicle entry extending into the vertebral body, indicating a focal increase along the screw path. Pedicle showed moderately elevated but more diffusely distributed stress along the pedicle axis. Lee and both LMS constructs maintained uniformly low-moderate levels, with Bi-LMS dispersing stress slightly more widely than Uni-LMS (Figs. 2 and 3).

Under axial rotation, PVMS values were 15.90 MPa (Lee), 43.22 MPa (Abumi), 14.73 MPa (Pedicle), 14.12 MPa (Uni-LMS), and 11.33 MPa (Bi-LMS). Abumi recorded the highest peak (43.22 MPa), with intense stress at the medial pedicle wall and entry site. Lee and Pedicle showed intermediate magnitudes with distribution over the posterior elements and lateral mass. Uni- and Bi-LMS yielded the lowest values and the most even distributions, with minimal concentration at cortical entry points (Fig. 2, Supplementary Fig. 2).

During lateral bending, the PVMS was 9.35 MPa (Lee), 27.07 MPa (Abumi), 8.23 MPa (Pedicle), 8.03 MPa (Uni-LMS), and 8.09 MPa (Bi-LMS). Abumi again exhibited the greatest concentration at the medial pedicle wall and entry zone. Lee demonstrated moderate stress around the posterior arch/lateral mass (bilateral red regions on the posterior view). Pedicle showed localized, moderate stress at the screw-bone interface. Uni-LMS had the most dispersed, low stress, while Bi-LMS presented a similarly low profile with slightly higher intensity at the far cortex (light-green zones) (Fig. 2, Supplementary Fig. 2).

Overall, across all 4 motions, Abumi consistently produced the largest PVMS (23.09–43.22 MPa) with focal concentrations at the pedicle entry and medial wall. LMS constructs—particularly Bi-LMS—showed the lowest magnitudes (8.03–11.33 MPa) with broad, uniform distributions. Lee and conventional Pedicle generally occupied an intermediate range with less intense focalization than Abumi.

2. PVMS at C6

At the C6 vertebral level, the PVMS was measured under the same motion conditions.

In flexion, PVMS values were 7.53 MPa (Lee), 24.96 MPa (Abumi), 6.21 MPa (Pedicle), 7.37 MPa (Uni-LMS), and 6.49 MPa (Bi-LMS). Abumi demonstrated the highest stress, concentrated along the medial pedicle wall and screw path, with vivid red zones consistent with the peak of 24.96 MPa. Lee technique showed moderate stress (7.53 MPa) at the lateral mass entry bilaterally. PSs displayed more centrally distributed stress along the screw-pedicle corridor (6.21 MPa), with linear red bands. Uni-LMS showed moderate, evenly spread stress without focal overload (7.37 MPa), while Bi-LMS exhibited slightly higher stress at the far cortex (6.49 MPa) but remained well distributed (Figs. 2 and 4).

In extension, the values were 7.55 MPa (Lee), 28.65 MPa (Abumi), 6.53 MPa (Pedicle), 7.40 MPa (Uni-LMS), and 7.02

 https://doi.org/10.14245/ns.2551470.735

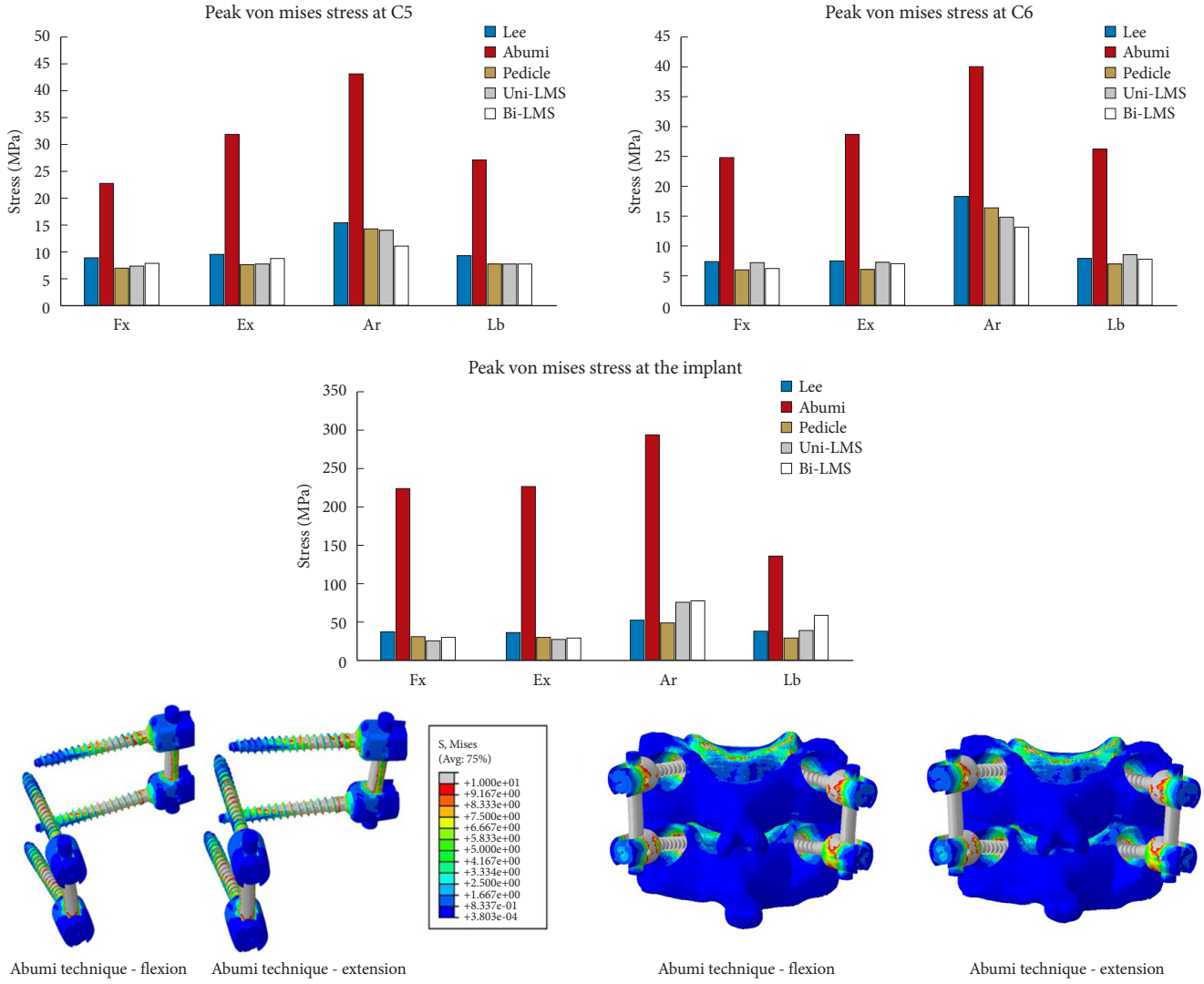

Fig. 2. Maximum von Mises stress (MPa) at the C5, C6 screw entry point and within the implant component under various loading conditions—flexion (Fx), extension (Ex), axial rotation (Ar), and lateral bending (Lb)—across 5 posterior fixation models: Lee technique, Abumi technique, conventional pedicle screw, unicortical lateral mass screw (Uni-LMS), and bicortical lateral mass screw (Bi-LMS). In the Abumi technique, a substantial portion of the lateral mass bone around the screw entry point is removed, resulting in markedly increased stress both on the surrounding bone and on the implant itself comparing to Lee technique or conventional technique. Illustrations of implant stress distribution for techniques other than the Abumi method are provided in the Supplementary Fig. 4.

MPa (Bi-LMS). Abumi again produced the highest stress, localized at the medial pedicle wall and entry point, with intense red zones in both axial and sagittal planes. Lee showed moderate stress at the lateral mass entry and posterior arch (7.55 MPa). PSs demonstrated diffuse stress distribution along the pedicle axis (6.53 MPa) without sharp focal overloads. Uni-LMS stress was concentrated mainly around the shaft (7.40 MPa), whereas Bi-LMS displayed slightly higher stress at the far cortex (7.02 MPa) but maintained a balanced distribution (Figs. 2 and 4).

In axial rotation, PVMS was 18.40 MPa (Lee), 39.91 MPa (Abumi), 16.58 MPa (Pedicle), 14.87 MPa (Uni-LMS), and 13.22 MPa (Bi-LMS). Abumi produced the greatest stress (39.91 MPa), with vivid red signals at the medial pedicle wall and screw entry zone. Lee (18.40 MPa) showed moderate stress distributed at the posterior arch and lateral mass entry. PSs (16.58 MPa) exhibited relatively uniform stress along the pedicle axis without focal overloads. Uni-LMS (14.87 MPa) showed localized but mild stress near the entry cortex, and Bi-LMS (13.22 MPa) revealed stress at the far cortex tip but otherwise low, diffuse distribution (Fig. 2, Supplementary Fig. 3).

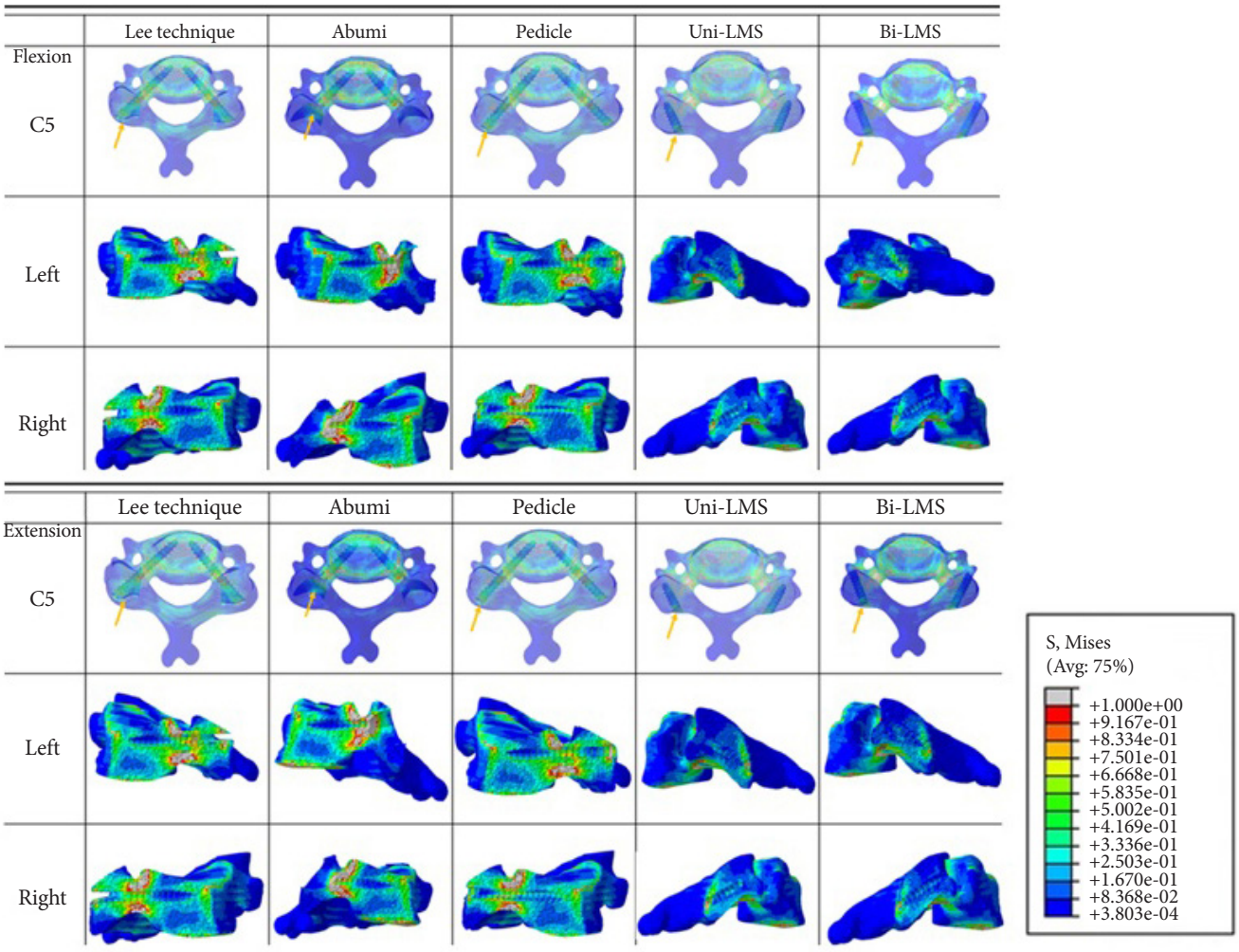

Fig. 3. Stress distribution during flexion and extension of C5; The yellow arrows indicate the regions with the highest stress, while the gray areas represent the zones of maximum stress concentration, as shown in the stress scale below. Abumi technique, stress during axial rotation and lateral bending was primarily concentrated around pedicle at the entry point. In contrast, for Lee technique and the conventional pedicle screw technique, stress was distributed across both the pedicle and around near cortex of lateral mass at the entry point. In the lateral mass screw technique, stress was also concentrated at the entry point. Stress distributions under axial rotation and lateral bending are provided in the Supplementary Fig. 2. Uni-LMS, unicortical lateral mass screw; Bi-LMS, bicortical lateral mass screw.

For lateral bending, the values were 7.99 MPa (Lee), 26.25 MPa (Abumi), 7.11 MPa (Pedicle), 8.43 MPa (Uni-LMS), and 8.01 MPa (Bi-LMS). Lee exhibited stress in the posterolateral lateral mass and pedicle, bilaterally extending along the screw axis. Abumi again showed the highest stress, concentrated at the medial pedicle and entry zone, especially on the right side. PSs demonstrated even distribution along the axis with moderate red zones (7.11 MPa). Uni-LMS showed lower stress overall (8.43 MPa), mainly at the lateral cortex, while Bi-LMS exhibited slightly deeper extension than Uni-LMS (8.01 MPa) but remained low in magnitude (Fig. 2, Supplementary Fig. 3).

Overall, across all 4 motions, the Abumi technique consistently yielded the highest PVMS at C6 (24.96–39.91 MPa), with focal overload at the pedicle entry and medial wall. In contrast, Uni- and Bi-LMS constructs showed the lowest stress magnitudes (6.49–14.87 MPa) with evenly distributed patterns. Lee and conventional Pedicle techniques generally occupied an intermediate range, with less intense focalization than Abumi but higher stress than LMS configurations.

3. PVMS at the Implant

The stress within the implant was assessed under the same 4 loading conditions.

Abumi technique showed the highest stress concentration,

https://doi.org/10.14245/ns.2551470.735

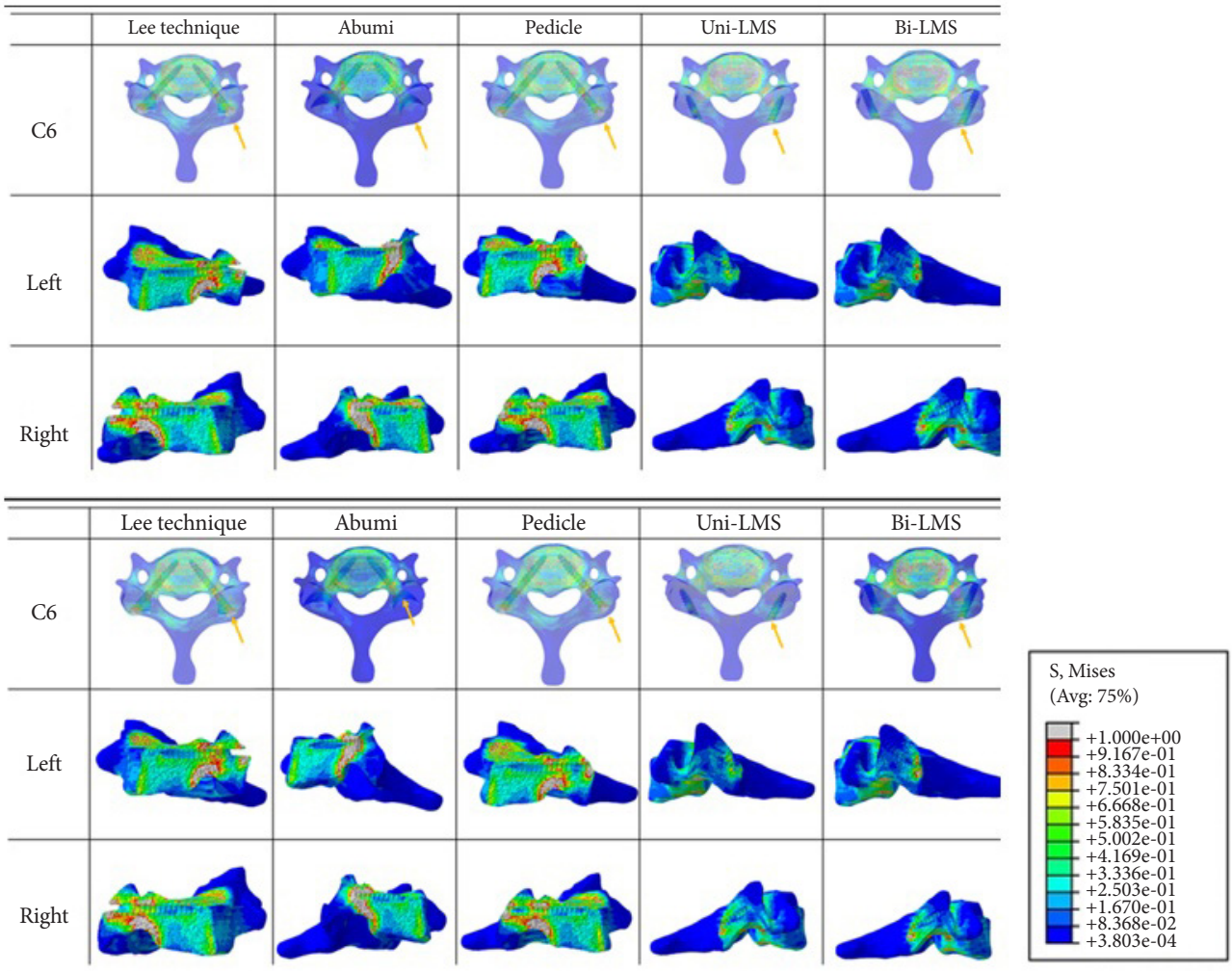

Fig. 4. Stress distribution during flexion and extension of C6; The yellow arrows indicate the regions with the highest stress, while the gray areas represent the zones of maximum stress concentration, as shown in the stress scale below. Abumi technique, stress during axial rotation and lateral bending was primarily concentrated around pedicle at the entry point. In contrast, for Lee technique and the conventional pedicle screw technique, stress was distributed across both the pedicle and around near cortex of lateral mass at the entry point. In the lateral mass screw technique, stress was also concentrated at the entry point. Stress distributions under axial rotation and lateral bending are provided in the Supplementary Fig. 3. Uni-LMS, unicortical lateral mass screw; Bi-LMS, bicortical lateral mass screw.

particularly along the shaft and screw head junction of the superior screws and rods. The intense red zones indicate substantial mechanical demand, consistent with the high PVMS values noted in earlier data (Fig. 2). Lee technique also demonstrated prominent stress along the screw neck and connecting rod, though to a lesser degree than the Abumi construct. Stress appeared symmetrically distributed between the upper and lower screws. PS fixation showed moderate stress localized around the middle shaft of the screw and along the rods, suggesting efficient load-sharing with less focal overload compared to Abumi (Supplementary Fig. 4). Unicortical LMSs presented with relatively low stress, with green to light yellow zones confined to the rod-screw junctions, indicating lower biomechanical demand across the construct. Bicortical LMSs exhibited slightly increased stress at the screw-bone interface compared to unicortical screws, but the implant body itself maintained low stress distribution overall.

In flexion, the PVMS reached 35.66 MPa (Lee), 225.56 MPa (Abumi), 29.91 MPa (Pedicle), 26.46 MPa (Uni-LMS), and 28.55 MPa (Bi-LMS). In extension, the values were 35.66 MPa (Lee), 226.89 MPa (Abumi), 29.91 MPa (Pedicle), 26.54 MPa (Uni-LMS), and 28.45 MPa (Bi-LMS). In axial rotation, the implant stress peaked at 51.79 MPa (Lee), 295.01 MPa (Abumi), 49.43 MPa (Pedicle), 76.5 MPa (Uni-LMS), and 77.97 MPa (Bi-

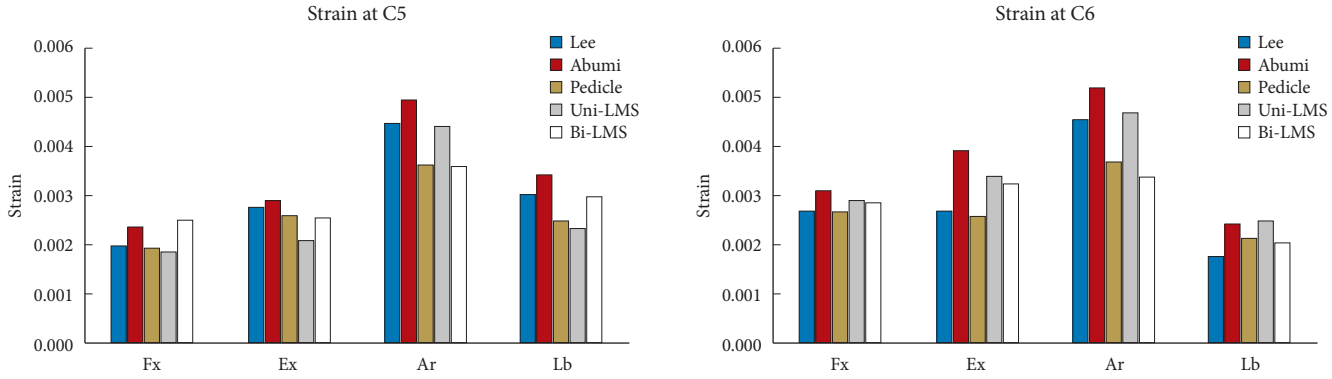

Fig. 5. Maximum principal strain at the C5, C6 vertebral body under flexion (Fx), extension (Ex), axial rotation (Ar), and lateral bending (Lb) across 5 posterior fixation techniques: Lee technique, Abumi technique, conventional pedicle screw, unicortical lateral mass screw (Uni-LMS), and bicortical lateral mass screw (Bi-LMS).

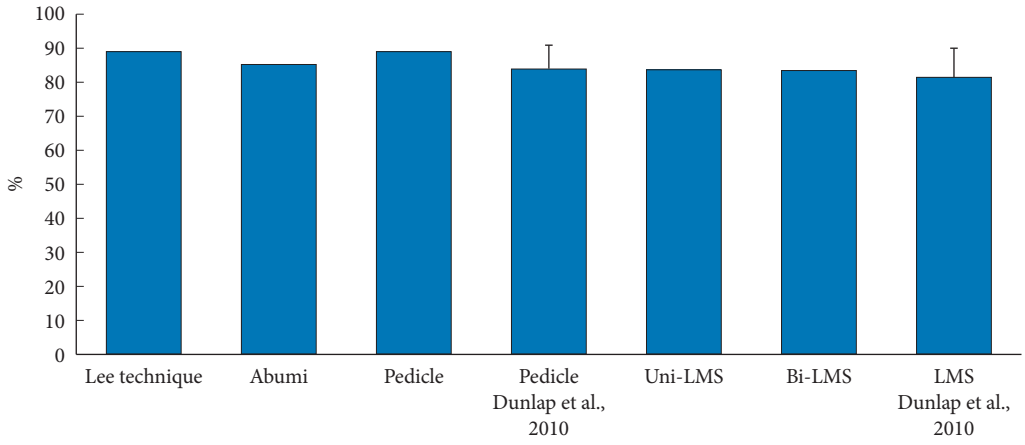

Fig. 6. Contribution of posterior load-sharing. Uni-LMS, unicortical lateral mass screw; Bi-LMS, bicortical lateral mass screw.

LMS). During lateral bending, values were 38.15 MPa (Lee), 136.68 MPa (Abumi), 27.58 MPa (Pedicle), 37.92 MPa (Uni-LMS), and 58.75 MPa (Bi-LMS) (Fig. 2).

4. Overall Strain Distribution

The Abumi technique consistently exhibited the highest vertebral strain at both C5 and C6, while LMS techniques resulted in lower strain distribution, indicating reduced local deformation and potential for cortical stress overload (Fig. 5).

The strain values at the C5 vertebral body were calculated under each motion condition. In flexion, the strain was 0.002001 (Lee), 0.002383 (Abumi), 0.001967 (Pedicle), 0.00187 (Uni-LMS), and 0.002502 (Bi-LMS). In extension, the values were 0.002765 (Lee), 0.002891 (Abumi), 0.002618 (Pedicle), 0.002096 (Uni-LMS), and 0.002539 (Bi-LMS). In axial rotation, strain values were 0.004509 (Lee), 0.004972 (Abumi), 0.003651 (Pedicle), 0.004397 (Uni-LMS), and 0.003621 (Bi-LMS). During lateral bending, the strain recorded was 0.00305 (Lee), 0.003406 (Abumi), 0.002477 (Pedicle), 0.002344 (Uni-LMS), and 0.003007 (Bi-LMS).

The strain values at the C6 vertebral body were calculated under each motion condition. In flexion, the strain was 0.002675 (Lee), 0.003107 (Abumi), 0.002665 (Pedicle), 0.002894 (Uni-LMS), and 0.002847 (Bi-LMS). In extension, the values were 0.002675 (Lee), 0.003922 (Abumi), 0.002563 (Pedicle), 0.003402 (Uni-LMS), and 0.003242 (Bi-LMS). In axial rotation, strain values were 0.004551 (Lee), 0.005196 (Abumi), 0.003672 (Pedicle), 0.004700 (Uni-LMS), and 0.003384 (Bi-LMS). During lateral bending, the strain recorded was 0.001754 (Lee), 0.002423 (Abumi), 0.002156 (Pedicle), 0.002491 (Uni-LMS), and 0.002016 (Bi-LMS).

5. Summary of PVMS Across All Techniques

To facilitate direct comparison among techniques, Table 1 summarizes the PVMS values for all 5 posterior fixation techniques (Lee point technique, Abumi technique, conventional

https://doi.org/10.14245/ns.2551470.735

Table 1. Summary of peak von Mises stress across all posterior cervical fixation techniques and loading conditions

(A) Peak von Mises stress at C5 vertebra (MPa)

Loading condition	Lee technique	Abumi technique	Pedicle screw	Uni-LMS	Bi-LMS
Flexion	9.14	23.09	7.51	7.80	8.03
Extension	9.57	31.96	8.19	7.82	8.63
Axial rotation	15.90	43.22	14.73	14.12	11.33
Lateral bending	9.35	27.07	8.23	8.03	8.09
Range (min–max)	9.14–15.90	23.09–43.22	7.51–14.73	7.80–14.12	8.03–11.33

(B) Peak von Mises stress at C6 vertebra (MPa)

Loading condition	Lee technique	Abumi technique	Pedicle screw	Uni-LMS	Bi-LMS
Flexion	7.53	24.96	6.21	7.37	6.49
Extension	7.55	28.65	6.53	7.40	7.02
Axial rotation	18.40	39.91	16.58	14.87	13.22
Lateral bending	7.99	26.25	7.11	8.43	8.01
Range (min–max)	7.53–18.40	24.96–39.91	6.21–16.58	7.37–14.87	6.49–13.22

(C) Peak von Mises stress at implant (MPa)

Loading condition	Lee technique	Abumi technique	Pedicle screw	Uni-LMS	Bi-LMS
Flexion	35.66	225.56	29.91	26.46	28.55
Extension	35.66	226.89	29.91	26.54	28.45
Axial rotation	51.79	295.01	49.43	76.50	77.97
Lateral bending	38.15	136.68	27.58	37.92	58.75
Range (min–max)	35.66–51.79	136.68–295.01	27.58–49.43	26.46–76.50	28.45–77.97

Uni-LMS, unicortical lateral mass screw; Bi-LMS, bicortical lateral mass screw.

PS, Uni-LMS, and bi-LMS) across all loading conditions at C5, C6, and the implant. As shown in Table 1, Abumi technique consistently produced the highest PVMS across all loading conditions and anatomical locations (bone: 23.09–43.22 MPa at C5, 24.96–39.91 MPa at C6; implant: 136.68–295.01 MPa). In contrast, LMS techniques (both unicortical and bicortical) generally exhibited the lowest and most uniform stress distributions (bone: 6.49–14.87 MPa; implant: 26.46–77.97 MPa). Lee point and conventional PS techniques showed intermediate stress levels with well-distributed patterns (bone: 7.51–18.40 MPa; implant: 27.58–51.79 MPa), suggesting a balanced biomechanical profile.

6. Validation of the FE Model

When the contribution of posterior load-sharing was compared with previous studies,[34] the load carried by the implant showed similar results across the different techniques. Furthermore, comparison with experimental data demonstrated that the predicted values fell within the corresponding standard deviation (Fig. 6, Supplementary Fig. 5).

DISCUSSION

1. Patient-Specific Material Properties and Model Development

In a previous cervical spine FE study, bone tissue is generally classified into cortical bone, cancellous bone, and posterior elements, with a single elastic modulus applied based on normal patient properties. However, such uniform material properties make it difficult to accurately reflect the clinical conditions of patients undergoing posterior fixation, since bone mineral density (BMD) varies across different regions. In particular, when evaluating the structural stability of posterior fixation techniques, the material properties of critical regions such as the pedicle and lateral mass, which are key factors in screw fixation strength, represent an even more significant limitation.

To address these limitations of previous studies, in the present study we constructed a cervical spine model with patient-

specific bony material properties derived from CT. As shown in Supplementary Fig. 6, the pedicle region demonstrated relatively higher material properties, while other regions were lower. Moreover, the bone at the PS fixation entry site was found to be denser, consistent with the characteristics of degenerative patients. This suggests that the patient-specific distribution of material properties provides a more realistic reflection of clinical experience.

Previous studies have shown that the mechanical properties of osteoporotic bone are reduced by approximately 20%–50% compared with normal bone.[35,36] In this study, as presented in Supplementary Table 1, the maximum material property was about 9,000 MPa, which corresponds to roughly 90% of the normal spine of 10,000 MPa. This indicates that the material properties of patients with osteopenia, the pre-stage of osteoporosis, were reflected in the model.

2. Biomechanical Findings and Stress Distribution Patterns

Although the Abumi technique is generally regarded as a safer approach due to its direct visualization and access to the pedicle, our analysis suggests that this technique results in notably higher stress concentrations around the screw entry point and along the screw shaft. From the perspective of Wolff's law, localized mechanical loading may enhance bone remodeling and promote fusion.[37] However, in the case of the Abumi technique, the magnitude of stress often exceeded the physiological threshold of cancellous bone. While this threshold may vary with bone density and anatomical site, a previous study identified 16.3 MPa as the upper limit of cancellous bone compressive strength,[38,39] which was adopted as the reference in this study. Stress values above this level suggest a potential risk of mechanical failure, including screw loosening or microfracture of the pedicle, particularly under repetitive loading. Implant stress values further support this concern, as maximum stresses in the Abumi model exceeded 200 MPa, indicating a high fatigue burden on the screw-rod construct.

In contrast, Lee point technique demonstrated a stress distribution pattern comparable to that of the conventional PS trajectory, suggesting that the biomechanical environment for bone fusion may not differ substantially between the two. Both demonstrated moderate stress around near cortex of lateral mass at the entry point and along the pedicle wall, without focal overload.

In PS models, stress consistently concentrated at the screw neck region. This finding aligns with clinical observations where screw breakage, when it occurs, typically initiates at the screw neck,[40] supporting the mechanical relevance of our FE predictions.

In LMS fixation models, stress was predominantly concentrated at the screw neck across all loading conditions. In the bicortical LMS configuration, screw fixation extended to the cortical surface at the screw tip, effectively lengthening the moment arm. This mechanical leverage increased torque transmission, thereby generating higher stress at the screw neck. Although bicortical fixation has traditionally been thought to offer biomechanical advantages due to cortical purchase and increased initial stability, recent studies have reported that bicortical LMS do not consistently demonstrate superior pullout strength compared to unicortical screws. Our results similarly suggest that the increase in stress concentration associated with bicortical LMS may elevate the risk of fatigue-related failure over time.[11,17,41]

Conversely, the unicortical LMS model showed relatively lower stress at the screw neck, which may be due to slight micromotions permitted within the surrounding cancellous bone. This subtle compliance may function as a mechanical buffer, reducing the magnitude of stress transmitted to the implant. Therefore, while unicortical fixation may offer less initial anchorage strength, it could be more favorable in terms of long-term mechanical endurance. However, even if fusion is accomplished, loosening is a known concern with LMSs, and the risk may be further increased when using unicortical fixation.[42,43]

3. Model Validation

We validated the FE model by applying pre-loads for each technique. However, previous studies[32,33] performed their experiments on the C4–5 or C6–7 motion segments rather than the C5–6 segment analyzed in the present study. This discrepancy may introduce slight differences in biomechanical behavior, which should be considered when comparing our results with those reported in the literature.

Although direct experimental validation using cadaveric or *in vitro* data was not performed, the overall stress and strain distributions of the present FE model were consistent with those reported in previous cervical spine FE studies. Specifically, the predicted range and localization of PVMS in the cortical bone and screw regions corresponded well with those in established models of C5–6 fixation.[21,22,44] The magnitude and direction of motion-dependent load transfer observed in this study were also comparable to prior cadaveric measurements of subaxial cervical motion segments.[32,33] As summarized in Supplementary Table 2, the stress magnitudes observed at the verte-

 https://doi.org/10.14245/ns.2551470.735

bral cortex and screw-bone interface in our study (6.21–43.22 MPa for bone, 26.46–295.01 MPa for implants) fell within the physiological ranges established by cadaveric experiments[32,33] and validated FE analyses.[21,22,44] These qualitative and quantitative agreements suggest that the present model provides a mechanically reasonable representation of posterior cervical fixation behavior.

In future study, we will integrate cadaveric studies and develop a multilevel FE model validated through biomechanical behavior analysis. This approach will allow us to improve the reliability of our findings by enabling prediction of not only the treated segment but the overall spinal segment as a whole.

4. Clinical Implications: Technique Selection

The biomechanical findings of this study have several practical implications for surgical decision-making in posterior cervical fixation, particularly in patients with compromised bone quality. In osteopenic or osteoporotic patients, as modeled in this study, the choice of fixation technique becomes critically important due to reduced bone strength and increased susceptibility to screw loosening or pullout. Our results suggest that Abumi's technique, despite its advantage of direct pedicle visualization, showed higher stress concentrations in osteopenic patients. The elevated stress values observed at the pedicle entry point and medial wall (23.09–43.22 MPa at C5, 24.96–39.91 MPa at C6)—exceeding the estimated cancellous bone yield threshold of approximately 16 MPa— indicate increased mechanical demand that may require careful consideration in patients with compromised bone quality, particularly during the early postoperative period before solid fusion is achieved. Therefore, in patients with degenerative or osteopenic bone conditions, alternative techniques that distribute stress more evenly may be biomechanically preferable.

Lee point technique and conventional PS fixation demonstrated intermediate stress levels (7.51–18.40 MPa) with well-distributed patterns, suggesting a more favorable balance between mechanical stability and bone preservation. The moderate stress magnitudes observed in these techniques may be sufficient to stimulate bone remodeling and promote fusion according to Wolff's law, while remaining below the threshold for mechanical failure.[45,46] This balanced stress profile makes these techniques potentially suitable for a broader range of patients, including those with mild to moderate osteopenia. However, in cases of severe osteoporosis or multilevel constructs requiring maximal initial stability, the slightly lower stress concentrations at critical interfaces may warrant consideration of supplementary anterior support or longer constructs to reduce motion at individual segments.

LMS techniques, both unicortical and bicortical, consistently produced the lowest stress magnitudes (6.49–14.87 MPa) with the most uniform distributions. While this may appear biomechanically advantageous in terms of reducing the risk of acute mechanical failure, the relatively low stress environment may be less optimal for stimulating robust bone-implant integration and fusion, particularly in osteoporotic bone where osteogenic capacity is already compromised. Additionally, the inherently limited bone purchase of LMSs compared to PSs raises concerns about long-term loosening, even after fusion is achieved. Therefore, LMS fixation may be most appropriate for patients with adequate lateral mass bone stock undergoing short-segment fixation with minimal expected long-term mechanical demands.

From the perspective of fusion success, the observed stress patterns provide insights into the mechanical environment conducive to bone healing. Moderate, evenly distributed stress—as seen with Lee point and conventional PS techniques—may represent a favorable mechanical stimulus for osteoblast activity and new bone formation at the graft-endplate interface. In contrast, higher focal stress (Abumi technique) may influence local bone remodeling patterns, while lower stress environments (lateral mass techniques) may provide different mechanical stimulation profiles for fusion. These considerations suggest that fusion rates and quality may vary among techniques, although clinical validation through comparative outcome studies remains necessary.

In the early postoperative period, before solid fusion provides biological stability, construct integrity depends entirely on mechanical fixation. The higher implant stress observed in the Abumi construct (136.68–295.01 MPa), particularly at the screw-rod junction and screw neck, indicates increased mechanical demand under repetitive loading, which may warrant consideration in patients with risk factors for delayed fusion such as smoking, diabetes, or other comorbidities. Conversely, the lower implant stress in LMS constructs (26.46–77.97 MPa) may offer improved resistance to hardware fatigue, although this must be weighed against the risk of screw loosening due to limited bone purchase.

In summary, our findings suggest a technique-selection algorithm based on patient-specific factors: (1) For patients with normal or mildly osteopenic bone, Lee point or conventional PS techniques offer a balanced biomechanical profile with moderate stress conducive to fusion; (2) For patients with se-

vere osteoporosis or concern for pedicle integrity, LMSs may reduce the risk of acute pedicle fracture, although consideration of anterior supplementation may be warranted; (3) Abumi technique, while offering direct visualization, showed higher localized stress concentrations that may warrant careful patient selection, particularly in those with compromised bone quality. These biomechanical insights, combined with individual anatomical considerations and surgical expertise, can inform evidence-based decision-making in posterior cervical fixation.

5. Limitations

This study has several limitations inherent to FE analysis. First, the material properties used in the model were assumed to be homogeneous, isotropic, and linearly elastic, which may not fully reflect the complex, anisotropic behavior of real human bone tissue—particularly in osteoporotic or elderly individuals. Second, while the boundary and loading conditions were designed to approximate physiological cervical spine motion, they may not fully capture the dynamic, multi-axial forces encountered *in vivo*. Third, soft tissue structures such as ligaments and muscles were not modeled in detail, potentially influencing the accuracy of load transfer and joint constraint behavior. Fourth, variations in surgical technique, bone quality, and implant insertion angle that occur in clinical practice were not included in the simulations, which may limit the generalizability of the results. Fifth, the assumed threshold of cancellous bone yield stress used for evaluating risk of failure may vary substantially depending on patient-specific factors such as BMD, sex, and age, which were not individually modeled in this study. Finally, while the stress distributions observed in this study were comparable to those reported in previously validated studies (as summarized in Supplementary Table 2), direct experimental validation using cadaveric specimens or *in vivo* measurements was not performed. Although such literature-based comparisons support the biomechanical plausibility of our model, direct experimental validation would provide additional confidence and further strengthen the findings.

Furthermore, this FE analysis was performed as a deterministic simulation based on a single patient-specific geometry and material property distribution. Repeated computational runs under identical boundary and loading conditions would yield identical PVMS results; therefore, statistical analysis (e.g., mean ± standard deviation or hypothesis testing) was not applicable. Instead, relative comparisons of stress magnitude and distribution among different fixation techniques were performed, which is consistent with the methodological approach adopted in previous spinal FE studies.[21,22,44] However, future studies incorporating patient-specific models from multiple individuals will be necessary to improve the generalizability of the present findings.

This study applied patient-specific material properties derived from a single female patient with osteopenia. Importantly, this patient profile reflects the typical surgical candidate population, as most patients requiring spinal surgery exhibit osteopenic or osteoporotic bone status. Recent epidemiological studies have demonstrated that approximately 70.8% of patients requiring spinal surgery present with at least osteopenia or osteoporosis,[47] with female patients comprising a disproportionately high percentage of this cohort (92.7% of females over 50 undergoing spine surgery have abnormal BMD).[48] Furthermore, the prevalence of osteoporosis and osteopenia in spine surgery patients has been reported as 34.2% and 43.5%, respectively, with significantly higher rates in females (43.0% osteoporosis, 31.6%–41.4% osteopenia) compared to males.[49,50] Therefore, the osteopenic female patient model employed in this study represents a clinically relevant and representative population for cervical posterior fixation procedures.

Nevertheless, this single-case analysis inherently introduces limitations regarding generalizability across individuals with different sex, BMD, and age. Compared with previous studies using normal or single, uniform material properties, our model likely represents a lower-bound estimate of the mechanical behavior relative to populations with normal or higher bone density. However, future studies incorporating patient-specific models from multiple individuals will be necessary to improve the generalizability of the present findings.

CONCLUSION

Abumi's technique, while offering direct visualization, showed higher localized stress concentrations that may warrant careful patient selection, particularly in those with compromised bone quality. In contrast, Lee point technique showed similar stress patterns to the conventional PS method while avoiding high-stress regions, suggesting it may offer a favorable biomechanical profile without compromising overall stability.

NOTES

Supplementary Materials: Supplementary Tables 1-2 and Supplementary Figs. 1-6 are available at https://doi.org/10.14245/ns.2551470.735.

Conflict of Interest: The authors have nothing to disclose.

Funding/Support: This study was supported by a new faculty research seed money grant of Yonsei University College of Medicine for 2025 (2025-32-0035).

Author Contribution: Conceptualization: BHL; Data curation: THP, SJL; Formal analysis: JS, WSJ, JWK, KSS; Funding acquisition: BHL; Methodology: THP, SJL, BHL; Project administration: BHL, JWK, KSS; Visualization: THP; Writing – original draft: JS, WSJ; Writing – review & editing: JS, WSJ, BHL.

ORCID

Joonoh Seo: 0000-0001-7969-7792
Woo-Seok Jung: 0009-0004-9813-7925
Tae Hyun Park: 0000-0002-9817-0176
Sung-Jae Lee: 0000-0001-5511-4839
Ji-Won Kwon: 0000-0003-4880-5310
Kyung-Soo Suk: 0000-0003-0633-2658
Byung Ho Lee: 0000-0001-7235-4981

REFERENCES

1. Oglesby M, Fineberg SJ, Patel AA, et al. Epidemiological trends in cervical spine surgery for degenerative diseases between 2002 and 2009. Spine (Phila Pa 1976) 2013;38:1226-32.
2. Passias PG, Poorman GW, Segreto FA, et al. traumatic fractures of the cervical spine: analysis of changes in incidence, cause, concurrent injuries, and complications among 488,262 patients from 2005 to 2013. World Neurosurg 2018;110:e427-37.
3. Duarte RM, Vaccaro AR. Spinal infection: state of the art and management algorithm. Eur Spine J 2013;22:2787-99.
4. Chachan S, Bin Abd Razak HR, Loo WL, et al. Cervical pedicle screw instrumentation is more reliable with O–arm–based 3D navigation: analysis of cervical pedicle screw placement accuracy with O–arm–based 3D navigation. Eur Spine J 2018; 27:2729-36.
5. Gan G, Kaliya-Perumal AK, Yu CS, et al. Spinal navigation for cervical pedicle screws: surgical pearls and pitfalls. Global Spine J 2021;11:196-202.
6. Lu S, Xu YQ, Lu WW, et al. A novel patient–specific navigational template for cervical pedicle screw placement. Spine (Phila Pa 1976) 2009;34:E959-66.
7. Joaquim AF, Tan L, Riew KD. Posterior screw fixation in the subaxial cervical spine: a technique and literature review. J Spine Surg 2020;6:252-61.
8. Lee YH, Abdou M, Kwon JW, et al. Posterior preventive foraminotomy before laminectomy combined with pedicle screw fixation may decrease the incidence of C5 palsy in complex cervical spine surgery in patients with severe myeloradiculopathy. J Clin Med 2023;12:2227.
9. Kim SH, Kim JH, Kwon JW, et al. Assessment of biomechanical advantages in combined anterior-posterior cervical spine surgery by radiological outcomes: pedicle screws over lateral mass screws. J Clin Med 2023;12:3201.
10. Suk KS, Jimenez KA, Jo JH, et al. Anterior plate-screws and lower postoperative T1 slope affect cervical allospacer failures in multi-level ACDF surgery: anterior versus posterior fixation. Global Spine J 2023;13:89-96.
11. Seybold EA, Baker JA, Criscitiello AA, et al. Characteristics of unicortical and bicortical lateral mass screws in the cervical spine. Spine (Phila Pa 1976) 1999;24:2397-403.
12. Richter M, Cakir B, Schmidt R. Cervical pedicle screws: conventional versus computer–assisted placement of cannulated screws. Spine (Phila Pa 1976) 2005;30:2280-7.
13. Abumi K, Itoh H, Taneichi H, et al. Transpedicular screw fixation for traumatic lesions of the middle and lower cervical spine: description of the techniques and preliminary report. J Spinal Disord 1994;7:19-28.
14. Abumi K, Shono Y, Ito M, et al. Complications of pedicle screw fixation in reconstructive surgery of the cervical spine. Spine (Phila Pa 1976) 2000;25:962-9.
15. Kwon JW, Arreza EO, Suguitan AA, et al. Medial pedicle pivot point using preoperative computed tomography morphometric measurements for cervical pedicle screw insertion: a novel technique and case series. J Clin Med 2022;11:396.
16. Heller JG, Estes BT, Zaouali M, et al. Biomechanical study of screws in the lateral masses: variables affecting pull–out resistance. J Bone Joint Surg Am 1996;78:1315-21.
17. Park CK, Hwang JH, Ji C. Comparisons of unicortical and bicortical lateral mass screws in the cervical spine: safety vs strength. J Korean Neurosurg Soc 2001;30:1210-9.
18. Ludwig SC, Kowalski JM, Edwards CC, et al. Cervical pedicle screws: comparative accuracy of two insertion techniques. Spine (Phila Pa 1976) 2000;25:2675-81.
19. Kowalski JM, Ludwig SC, Hutton WC, et al. Cervical spine pedicle screws: a biomechanical comparison of two insertion techniques. Spine (Phila Pa 1976) 2000;25:2865-7.
20. Jo DJ, Seo EM, Kim KT, et al. Cervical pedicle screw insertion using the technique with direct exposure of the pedicle by laminoforaminotomy. J Korean Neurosurg Soc 2012;52: 459-65.
21. Duan Y, Wang HH, Jin AM, et al. Finite element analysis of posterior cervical fixation. Orthop Traumatol Surg Res 2015;

101:23-9.
22. Ito Z, Higashino K, Kato S, et al. Pedicle screws can be 4 times stronger than lateral mass screws for insertion in the mid-cervical spine: a biomechanical study on strength of fixation. J Spinal Disord Tech 2014;27:80-5.
23. Kulkarni AG, Kumar P, Shetty GM, et al. Finite element analysis comparing the biomechanical parameters in multilevel posterior cervical instrumentation model involving lateral mass screw versus transpedicular screw fixation at the C7 vertebra. Asian Spine J 2024;18:163-73.
24. Harinathan B, Jebaseelan D, Yoganandan N, et al. Comparing adjacent segment biomechanics between anterior and posterior cervical fusion using patient–specific finite element modeling. Asian Spine J 2024;18:777-93.
25. Pitzen T, Geisler F, Matthis D, et al. A finite element model for predicting the biomechanical behaviour of the human lumbar spine. Control Eng Pract 2002;10:83-90.
26. Son DM, Lee SB, Lee SJ, et al. Biomechanical comparison of multilevel lumbar instrumented fusions in adult spinal deformity according to the upper and lower fusion levels: a finite element analysis. Biomed Res Int 2022;2022:2534350.
27. Hong JB, Son DM, Park TH, et al. Risk of rod fracture according to cross-link position in pedicle subtraction osteotomy (PSO): a finite element study. J Clin Neurosci 2020;73:304-7.
28. Taddei F, Schileo E, Helgason B, et al. The material mapping strategy influences the accuracy of CT–based finite element models of bones: an evaluation against experimental measurements. Med Eng Phys 2007;29:973-9.
29. Ciarelli MJ, Goldstein SA, Kuhn JL, et al. Evaluation of orthogonal mechanical properties and density of human trabecular bone from the major metaphyseal regions with materials testing and computed tomography. J Orthop Res 1991;9:674-82.
30. Rho JY, Hobatho MC, Ashman RB. Relations of mechanical properties to density and CT numbers in human bone. Med Eng Phys 1995;17:347-55.
31. Lee S, Lee H, Park T, et al. Biomechanical comparison of posterior fixation combinations with an allograft spacer between the lateral mass and pedicle screws. Appl Sci 2020;10:7291.
32. Panjabi MM, Crisco JJ, Vasavada A, et al. Mechanical properties of the human cervical spine as shown by three–dimensional load–displacement curves. Spine (Phila Pa 1976) 2001;26:2692-700.
33. Moroney SP, Schultz AB, Miller JA, et al. Load-displacement properties of lower cervical spine motion segments. J Biomech 1988;21:769-79.
34. Dunlap BJ, Karaikovic EE, Park HS, et al. Load sharing properties of cervical pedicle screw-rod constructs versus lateral mass screw-rod constructs. Eur Spine J 2010;19:803-8.
35. Zioupos P, Currey JD. Changes in the stiffness, strength, and toughness of human cortical bone with age. Bone 1998;22:57-66.
36. Augat P, Schorlemmer S. The role of cortical bone and its microstructure in bone strength. Age Ageing 2006;35 Suppl 2:ii27-31.
37. Frost HM. Wolff's Law and bone's structural adaptations to mechanical usage: an overview for clinicians. Angle Orthod 1994;64:175-88.
38. Kopperdahl DL, Morgan EF, Keaveny TM. Quantitative computed tomography estimates of the mechanical properties of human vertebral trabecular bone. J Orthop Res 2002;20:801-5.
39. Fyhrie DP, Vashishth D. Bone stiffness predicts strength similarly for human vertebral cancellous bone in compression and for cortical bone in tension. Bone 2000;26:169-73.
40. Stanford RE, Loefler AH, Stanford PM, et al. Multiaxial pedicle screw designs: static and dynamic mechanical testing. Spine (Phila Pa 1976) 2004;29:367-75.
41. Harris BM, Hilibrand AS, Nien YH, et al. A comparison of three screw types for unicortical fixation in the lateral mass of the cervical spine. Spine (Phila Pa 1976) 2001;26:2427-31.
42. Røhl L, Larsen E, Linde F, et al. Tensile and compressive properties of cancellous bone. J Biomech 1991;24:1143-9.
43. Kopperdahl DL, Keaveny TM. Yield strain behavior of trabecular bone. J Biomech 1998;31:601-8.
44. Tan LA, Yoganandan N, Choi H, et al. Biomechanical analysis of 3-level anterior cervical discectomy and fusion under physiologic loads using a finite element model. Neurospine 2022;19:385-92.
45. Frost HM. From Wolff's law to the Utah paradigm: insights about bone physiology and its clinical applications. Anat Rec 2001;262:398-419.
46. Pilitsis JG, Lucas DR, Rengachary SS. Bone healing and spinal fusion. Neurosurg Focus 2002;13:e1.
47. Schmidt T, Ebert K, Rolvien T, et al. A retrospective analysis of bone mineral status in patients requiring spinal surgery. BMC Musculoskelet Disord 2018;19:53.
48. Sardar Z, Coury J, Polly D, et al. Osteoporosis in adult patients undergoing spinal reconstructive surgery: associated complications and management. Global Spine J 2025;15(3_suppl):61S-74S.

 https://doi.org/10.14245/ns.2551470.735

49. Fan ZQ, Yan XA, Li BF, et al. Prevalence of osteoporosis in spinal surgery patients older than 50 years: a systematic review and meta-analysis. PLoS One 2023;18:e0286110.
50. Chin DK, Park JY, Yoon YS, et al. Prevalence of osteoporosis in patients requiring spine surgery: incidence and significance of osteoporosis in spine disease. Osteoporos Int 2007;18:1219-24.